
Article:
Pravinata, LC and Murray, BS orcid.org/0000-0002-6493-1547 (2019) Encapsulation of water-insoluble polyphenols and β-carotene in Ca-alginate microgel particles produced by the Leeds Jet Homogenizer. Colloids and Surfaces A: Physicochemical and Engineering Aspects, 561. pp. 147-154. ISSN 0927-7757

https://doi.org/10.1016/j.colsurfa.2018.10.041

Encapsulation of water-insoluble polyphenols and β-carotene in Ca-alginate microgel particles produced by the Leeds Jet Homogenizer

Linda C. Pravinata and Brent S. Murray*

* Author for correspondence

b.s.murray@leeds.ac.uk

Abstract

Polyphenols and β-carotene are widely studied due to their perceived multiple health functions, but their poor solubility in water inhibits their addition to foodstuffs. This provides a motivation for this study: to entrap these water–insoluble compounds into Ca-alginate microgel particles prepared via a special technique termed the Leeds Jet Homogenizer. Water-insoluble particles of polyphenols and β-carotene were successfully loaded into the microgel particles as revealed by images obtained from confocal laser scanning microscopy (CLSM). Microgel particles were separated via incorporation of magnetic nanoparticles (MNPs) into the particles and application of a magnetic field or via centrifugation, to quantify the yield, payload, and loading efficiencies. It was found that microgel particle yields improved on introducing these water-insoluble compounds up to 10 % to 30 %. The payloads of compounds in the particles were only < 1.5 % but mainly due to the low initial concentrations were used, i.e. 0.5 and 18.5 mM for polyphenols and β-carotene, respectively. The loading efficiencies were considerably high, i.e. between 21 to 58 %. In short, the results show firm evidence that useful encapsulation of such water-insoluble compounds within Ca-alginate microgel particles can be achieved via this simple and effective technique.

Keywords: encapsulation, alginate, microgels, polyphenols, curcumin, β-carotene

1. Introduction

Encapsulation technology is undergoing continuous research and development, due to its ability to enhance the availability of bioactive or functional ingredients. It helps to protect the encapsulated compounds to reach the desired sites for a controlled release, either via fragmentation, erosion, diffusion or swelling of the encapsulating entity.[1] Microgel particles can offer a perfect vehicle to deliver such functions, encapsulating a variety of compounds ranging from small molecules, solid particles or liquid droplets, structured micelles or vesicles and so on.[2] Emulsion filled microgel particles are one of the examples of these filled microgels that have recently been reviewed as a way to deliver lipophilic molecules.[2]

Polyphenols have been widely studied for their potential health benefits as antioxidants, anti-cancer agents, immunomodulatory effects, etc.[3-5] Therefore, entrapping them in water-dispersible microgel particles could be beneficial as a means to increase their incorporation into foodstuffs and control their uptake. In addition to the aforementioned protection benefits of nano- or microencapsulation, encapsulation can also aid in masking unpleasant tastes.[6] Phenolic compounds are known to be intrinsically bitter, thus encapsulating them in microgel particles can be beneficial for food applications. Moreover, ease of dissolution in hydrophilic beverage systems can also be achieved via formation of small microgel particle sizes; particle sizes of < 20 nm can easily be dispersed to create transparent beverages.[7] A top priority in developing foods or supplements that are enriched with the health-promoting phytochemicals are continuous production methods. The most recent developments of nano- and microencapsulation agents as delivery systems have been comprehensively reviewed by Souza et al.[8]

The aim of this study is to explore the possibilities of entrapping water-insoluble compounds such as flavonoids (rutin and tiliroside), curcumin and β-carotene into Ca-alginate microgel particles produced via the Leeds jet homogenizer. The detailed principles of this method have been described previously by Pravinata et al.[9] The solubility limits of tiliroside, rutin, and curcumin in water are 2.1 μM at pH 8, ~0.1 mM, and 0.25 mM at pH 8, respectively.[10-13] Rutin has a sugar moiety attached to the flavonol structure as shown in Figure 1 which contributes to higher solubility compared to tiliroside.[11] The concentration of polyphenols used in this study, i.e.,

0.5 mM, is way above the solubility limit (in water) of these compounds, which are therefore largely present as insoluble organic crystals. The oil soluble isoprenoid compound of β-carotene (see Figure 1) has a high melting point of 178 °C.[14] Thus, it should also be in the crystalline form under the experimental conditions of the current study, which was conducted at room temperature (20 ± 4 °C).

2. Materials and Methods

2.1. Materials

Alginic acid, sodium salt, low viscosity (LV), rutin trihydrate 97%, and curcumin 95 % from Turmeric rhizome were purchased from AlfaAesar (Heysham, UK). Calcium chloride dihydrate (99.5%, Lot 81K0252), sodium azide (99.5%), β-carotene, (>97%), Tween 20, gelatin from bovine skin, FITC-dextran (M_w = 2x10^3 kDa., Lot SLBB6384V) and imidazole were sourced from Sigma Chemicals, St. Louis, MO , USA and were used as received. Tiliroside was purchased from RonaCare®. The pH of imidazole buffer was adjusted with 0.5 mol dm^{-3} HCl solution (Convol, BHD Chemicals Poole, UK) and 1 mol dm^{-3} NaOH (Fisher Scientific UK) using Jenway 3310 pH meter (Jenway, Essex, UK). Water, purified by a MilliQ apparatus (Millipore, Bedford, UK) with a resistivity greater than 18.2 MΩ.cm, was used for the preparation of all solutions. For extraction of the water-insoluble compounds above, they were dissolved in 99.99% ethanol (ρ = 0.79 kg.L^{-1}) manufactured by VWR Internationals (Fontenay-sous-Bois, France). The chemicals to produce the magnetic particles were iron III hexahydrate (from Sigma-Aldrich Co, St. Louis, MO, USA), iron II chloride tetrahydrate (from Acros Organics, NJ, USA), and ammonia solution, 35 %, specific gravity = 0.88 (from Fischer Scientific, Loughborough, UK). A high performance Neodymium magnet (First Magnets®, Nottinghamshire, UK) with 28 mm dia. x 11 mm thick coated with PTFE Teflon (manufactured by from Magnet Experts Ltd, Newark, UK) was used to collect the magnetic nanoparticles and the encapsulated microgel particles.

2.2. Encapsulation of water insoluble materials into Ca-alginate microgel particles via the Leeds Jet Homogenizer

The method of producing the microgel particles has been explained in detail previously by Pravinata et al.[9] and so the main details here refer to encapsulation of insoluble materials into these particles and their characterization. To incorporate the water-insoluble particles, 1 mM concentrations of the insoluble polyphenols and 37 mM of β-carotene (with or without Tween 20) were mixed into 25 ml of Millipore water using IKA Labortechnik Ultraturrax T25 S7 (Janke & Kunkel GmbH & Co, Funkentstort, Germany) at 24,000 rpm for 2 minutes. The suspension was then mixed with 4 wt.% alginate stock solution at 1:1 wt. ratio. At this stage, if used, magnetic nanoparticles (MNPs) with a concentration of 0.02 wt.% wet weight basis was spiked into the alginate phase. The MNPs were produced via mixing $FeCl_2$ and $FeCl_3$ in the presence of ammonia solution as a reducing agent.[15] The solid content at the MNPs was 0.19 ± 0.01 wt.% and particle size was 133.9 ± 1.2 nm, measured via the Malvern Zeta Nano-ZS (see below). Mild sonication was applied to the suspension of alginate + insoluble materials for encapsulation (with or without the MNPs) using a PUL 55 sonicator (Kerry Ultrasonic Ltd., Hertfordshire, UK) for 5 minutes to remove any air bubbles. The final mixture contained 2 wt.% alginate and the concentrations of encapsulated materials were 0.5 mM for the insoluble polyphenols and 18.5 mM for the β-carotene with or without 3 wt.% Tween 20. The mixture was then placed in one block of the jet homogenizer and 20 mM $CaCl_2$ in the other block. The jet homogenizer forces the contents of the two blocks through a narrow jet at highly velocity, resulting in extremely rapid and turbulent mixing and in this case micron-sized calcium alginate microgel particles.[16] In this work the ratio of the volume of alginate-containing block to the $CaCl_2$-containing block was 4:1 and these materials were forced through the jet at 300 bar. The same technique has been recently used to produce starch[17], soy protein[18], whey protein microgel[19], and emulsion microgel particles[16] in which the latter gives a further analysis of the hydrodynamic conditions in the jet homogenizer that lead to microgel particle formation.

2.3. Spectrophotometric analysis of encapsulated materials

Standard absorbance versus concentration curves of the flavonoids and β-carotene in ethanol were generated for each compound of interest. Absorbance was measured via a Jenway 6715 spectrophotometer

96 (Bibby Scientific Ltd, Staffordshire, UK). The peak absorbance was collected at wavelengths of 360 nm for rutin,
97 325 nm for tiliroside, 420 nm for curcumin, and 450 nm for β-carotene. A linear correlation line with $R^2 > 0.98$
98 was obtained for each compound (with or without zero intercept, the R^2 values are similar, >0.98). The
99 absorbance of the microgel particles containing no encapsulated materials were also measured (since they had a
100 slight yellow appearance), but they resulted close to equivalent zero concentration.

101 To quantify the encapsulated compounds entrapped in the microgel particles, particles containing the added
102 MNPs were magnetically separated from the aqueous phase by placing a strong magnet on the side of the
103 beaker containing the suspension and draining off the aqueous solution. The remaining material was then mixed
104 with a known volume of ethanol for 30 min to dissolve the encapsulated compounds out of the particles.
105 (Generally about 50 µl of the harvested microgel particles was extracted with 5 ml of ethanol). The mixture was
106 then filtered using *Fisher*brand filter paper (Fisher Scientific, Loughborough, UK) grade 111 to remove microgel
107 particle material and 1 ml of the filtered ethanol solution was placed in a PMMA cuvette and the absorbance
108 measured. Via the standard curve and any appropriate dilution with ethanol applied, the absorbance was
109 converted concentration.

110 *2.4. Particle size and surface charge measurements*

111 The size distribution of the microgel particles, with or without encapsulated materials, was measured via
112 a Malvern Mastersizer 3000E Hydro, (Malvern Instruments, Worcestershire, UK). The refractive index of the
113 continuous phase (water) was taken as 1.33. It is difficult to know what refractive index to take for the microgel
114 particles, which will depend on the mean concentration of alginate within them plus the concentration of any
115 encapsulated material they contain. However, on varying the refractive index from 1.45 to 2.42, it was found that
116 the particle size distribution (*PSD*) was insensitive to these changes, within experimental error. The obscuration
117 range was set at 1 – 4 % and absorption index from 0.01 to 0.1.

118 The particle size distribution (*PSD*) of the water-insoluble crystals was measured via a Zetasizer Nano-
119 ZS (Malvern instruments, Worcestershire UK). The samples were filtered through 1 µm Whatman filter to remove

120 any large aggregates or dust (Malvern Instruments, 2011). The samples were placed in disposable PMMA
121 cuvettes and the *PSD* measured at 25°C, detecting scattered light at 173°. The ζ-potential of the microgel
122 particles was also measured via the same instrument, placing the samples in folded capillary electrophoresis cells
123 DTS1061 (Malvern, Worcestershire, UK). Measurements were made in triplicate and electrophoretic mobilities
124 converted to ζ-potentials via the Smoluchowski approximation.

125 *2.5. Confocal Laser Scanning Microscopy (CLSM) Method*

126 For samples intended for CLSM experiments, 4 wt.% gelatin was dissolved in water at 35°C with stirring,
127 for up to 30 min, then the microgel suspension mixed with the gelatin solution at a 1:1 weight ratio. FITC-dextran
128 was added at a concentration of 0.2 wt.% to the mixture of microgel + gelatin and a sample of this mixture placed
129 into a welled slide 30 mm in diameter and 3 mm deep, then covered with a coverslip. The slide was then placed
130 in a refrigerator and left overnight to solidify. The gelatin thus immobilizes any microgel particles in the aqueous
131 phase and aids their imaging. A Leica TCS SP2 Confocal Microscope used (Leica Microsystems, Manheim,
132 Germany) to image the samples, using Ar/ArKr (488, 514 nm) laser source and 40x oil immersion lens. A drop of
133 immersion liquid type F with refractive index of 1.518 (Leica Microsystem CMS Gmbh, Wetzlar, Germany) placed
134 on the cover slip to enhance the resolution. Two PMT detectors were activated simultaneously to detect signals
135 from two different fluorophores: the polyphenol (or β-carotene) and FITC-dextran at different emission bands, so
136 that both the encapsulated crystals and microgel particles could be visualized in situ. The excitation wavelengths
137 for the polyphenols, β-carotene, and FITC-dextran were set at 488, 458, and 514 nm, respectively. Emission
138 signals were collected from 460 to 480 nm for the polyphenols and from 530 to 580 nm for β-carotene. The FITC-
139 dextran emission was collected between 500 and 550 nm in samples containing polyphenols and between 490
140 and 510 nm for β-carotene containing microgel particles, to avoid any interference of the signals.

141 *2.6. Statistical Analysis*

142 All the experiments were performed in triplicate with the mean value and standard deviation expressed as the
143 error bars unless stated otherwise. The difference in mean values were analysed using SPSS (IBM Statistics 22
144 SPSS). Significant differences were reported as $p < 0.05$ using the student's t-test and ANOVA. The correlation
145 factor was determined using Pearson's test.

146 **3. Results and Discussion**

147 *3.1. Particle size of the microgel particles and the polyphenol compounds*

148 Microgel particles were produced at pH 5 and 8 in 0.02 M imidazole buffer (see Figure 2). At pH 8, the *PSD*
149 displayed a broad monomodal peak ranging between 1 and 250 µm plus a peak at around 30 µm. At pH 5, the
150 *PSD* was bimodal distribution with peaks at around 10 µm and 100 µm. In general, most microgel particle sizes
151 were below 300 µm at both pHs. The *PSD*s of the insoluble polyphenol compounds were between 0.1 to 100
152 µm, as also shown in Figure 2. Tiliroside possessed the smallest particle size with peaks at around 0.3 µm and 1
153 µm while curcumin had the broadest *PSD* (peaks at around 10 µm and 100 µm), whilst rutin had a *PSD* with a
154 peak at ca. 20 µm. Note these *PSD*s were obtained by dispersing them in MilliQ water (pH 6.8 ± 0.2) via the
155 Ultraturrax at 24,000 rpm *without* passing through the jet homogenizer. It is unsurprising to find them in
156 aggregated forms, whereas passage through the jet homogenizer might break up such aggregates to some
157 extent. Apparently there were also some nanocrystals of polyphenols present, as measured via Zetasizer with Z-
158 averages (μ_z) of, from the smallest to the largest, 182 nm for tiliroside, 211 nm for rutin and 217 nm for curcumin.
159 The combination of such broad size distributions of the microgel particles with the much smaller sizes of the
160 polyphenol crystals was expected to aid entrapment of most of the water-insoluble material.

161 The Sauter mean diameter ($d_{3,2}$) of the microgel particles with and without the entrapped polyphenols at
162 pH 5 and 8 is displayed in Figure 3a. The $d_{3,2}$ of these microgel particles with encapsulated polyphenols followed
163 the same size order as the μ_z of the nanocrystals of polyphenols. Tiliroside, with the smallest nanocrystals, gave
164 the smallest $d_{3,2}$ in the encapsulated form (Ca-ALG+T) with values of around 3.4 µm and 0.1 µm at pH 5 and 8,
165 respectively. The nanocrystals of rutin and curcumin were roughly around the same and the $d_{3,2}$ for both in

166 encapsulated forms (abbreviated as Ca-ALG+R and Ca-ALG+CU, respectively) also reflected the same size
167 range. The $d_{3,2}$ of Ca-ALG+CU and Ca-ALG+R were around 8 μm at pH 5 and 11 μm at pH 8 with higher mean
168 diameter at higher pH. Thus, the size of polyphenol nanocrystals might influence the final size of the entrapped
169 microgel particles, possibly via them acting like "nuclei" during the formation of the microgel particles.
170 As observed, there was an effect of pH on the microgel particle mean diameter:
171
172 The $d_{3,2}$ for the microgel particles without polyphenols (Ca-ALG Blank) was smaller at pH 5 than pH 8
173 (see Figure 3a): $d_{3,2}$ values for the Ca-ALG Blank were 5.0 ± 0.5 μm and 7.3 ± 1.0 μm at pH 5 and 8,
174 respectively. The shrinkage of Ca-ALG BLANK at low pH was probably due to the loss of electrostatic repulsion
175 between COO^- groups in alginate chains in the presence of abundantly available H^+ ions.[20] With the pK_a of the
176 COO^- groups approximately 3.5, the microgel particles are inclined to be more swollen at higher pH due to mutual
177 repulsion between the negatively charged chains and greater uptake of water.[21-22]
178 The $d_{3,2}$ of microgel particles with encapsulated curcumin (Ca-ALG+CU) was smaller at pH 5 , i.e., 7.8 ±
179 3.5 μm, compared to pH 8, i.e., 11.4 ± 5.8 μm, although the difference was not significant (with $p > 0.05$ due
180 large standard deviation for both pHs, see Figure 3a). The average net charge of curcumin at different pHs was
181 reported by Wang et al.[23] in their Supporting document, by taking into account of each of the functional groups
182 in the curcumin structure. The pK_a of the keto-enol group was 8.4, and that of both phenol groups were 9.9 and
183 10.5. At the pH values used here, the net charge of curcumin would be zero at pH 5 and slightly less than zero (~-
184 0.25 net charge) at pH 8. The lack of difference in $d_{3,2}$ of Ca-ALG+CU is thus supported by the lack of difference
185 in average net charge of curcumin at both pH 5 and 8.
186 The $d_{3,2}$ of microgel particles with encapsulated rutin (Ca-ALG+R) at pH 5 were smaller than at pH 8, i.e.
187 8.5 ± 1.2 μm vs. 11 ± 2.3 μm ($p < 0.05$). The pKa of the OH group in the C_7 location of the flavone ring of rutin is
188 ~7.1, which is therefore prone to changes in dissociation between pH 4 and 8.[24] Thus, at pH 8 there would be
189 an increase in electrostatic repulsion between negatively charged rutin and dissociated carboxyl groups in the
190 alginate chains, which might be expected to lead to larger particle size. By the same token, at pH 5, the Ca-

191 ALG+R particles may have become smaller due to attractive forces between slightly positively rutin and
192 negatively charged alginate.

193 Microgel particles with encapsulated tiliroside (Ca-ALG+T) behaved differently. Ca-ALG+T exhibited
194 significantly smaller sizes at pH 8 compared to pH 5; $d_{3,2}$ were 3.4 ± 0.3 μm and 0.1 ± 0.01 μm, respectively (see
195 Figure 3a). Luo et al.[11] measured the particle size and ζ-potential of tiliroside crystals in imidazole buffer from
196 pH from 2 to 8 in the presence of 0.05 M NaCl (there was no added NaCl in this current study, but the presence
197 of salt is not expected to impact the ζ-potential values significantly). Their results showed an increase in tiliroside
198 particle size when the ζ-potential changed from negative to positive at lower pH. The increase of particle radius of
199 tiliroside was more pronounced as its ζ-potential was close to zero. They postulated that at low pH the tiliroside
200 has a tendency to form intermolecular aggregates which caused the particle size to be larger. This could be key
201 to understanding why Ca-ALG+T particle size was larger at pH 5 vs. pH 8. Perhaps the entrapment occurs when
202 the tiliroside crystals are still in aggregated form at pH 5. Although at pH 5 the ζ -potential of tiliroside was not
203 zero, but around –10 mV, the particle size of tiliroside at pH 5 was at least 50 % larger than at pH 8.[11] The jet
204 homogenizer is known to provide a very rapid mixing, but apparently it still cannot prevent this tiliroside
205 aggregation, i.e., tiliroside aggregate formation must occur at a faster timescale compared to the reaction time of
206 Ca-alginate bridging, thus aggregates of tiliroside crystals are entrapped.

207 Figure 3b shows the ζ-potential of the microgel particles with or without flavonoids at pH 5 and 8. All
208 these microgel particles exhibited less negative values at pH 5 compared to pH 8, which suggests the effect of pH
209 on the dissociation of the alginate carboxylates dominates. At both pHs, the ζ-potentials of Ca-ALG+R and Ca-
210 ALG+T tended to be more negative compared to Ca-ALG Blank. This suggests that significant amounts of rutin
211 and tiliroside present at the surface of the microgel particles. The ubiquitous presence of OH functional groups in
212 polyphenols could be mainly responsible for the adsorption to the microgel particles, either via Ca^{2+} cross-linking
213 or hydrogen bonding interactions.[11]

214 *3.2. Particle size of β-carotene encapsulated microgel particles*

215 Figure 4 shows the particle size of β-carotene (BC) crystals in the presence of Tween 20 (TW20) and in
216 its encapsulated form in the microgel particles (Ca-ALG+BC+TW20). The initial coarse dispersion of BC in water
217 had a broad PSD centred on 5.4 ± 2.6 μm. As it was dispersed into the alginate phase (2 wt.% alginate
218 concentration) before passing through the jet homogenizer, the PSD shifted to larger sizes, with the distribution
219 centred on a peak at 15.4 μm. This increase in size is probably due to depletion flocculation when mixing the
220 polymer with the BC. A similar phenomenon was observed when BC oil droplets were mixed with mucin during an
221 in vitro digestion study.[25] These workers found an enlargement of the mean droplet size of BC in the mouth and
222 stomach during the early onset of digestion and attributed it to the high molecular weight mucins present.
223 Although there was some size increase on mixing with alginate, after passing through the jet homogenizer the
224 mean size of Ca-ALG+BC+TW20 system reverted back to close to the original BC crystal size of ~5.5 μm.
225 Whether or not this size refers to free or encapsulated BC (see Figure 4), this illustrates the ability of the jet
226 homogenizer to break flocs of these organic crystals into smaller sizes.

227 *3.3. Examination of effect of MNPs on encapsulation of materials into microgel particles*

228 Checks were also performed to confirm that addition of the MNPs also did not influence the size of the
229 microgel particles with or without BC or polyphenols. The average of $d_{3,2}$ of BC + TW20 encapsulated in microgel
230 particles with or without the MNPs were similar, i.e., 4.91 ± 0.12 μm and 5.44 ±0.49 μm, respectively (data not
231 shown) and the peak in the *PSD* showed no significant shift as the MNPs were added into the Ca-
232 ALG+BC+TW20 system. This implied minimal interaction of MNPs with the microgel particles or β-carotene.
233 Polyphenols are known to chelate metal ions via negatively charged hydroxyl groups which can bind the
234 positively charged metal ions so it was also important to check that the MNPs did not affect the formation of the
235 microgel particles or encapsulation of polyphenols within them. The ζ-potential of the MNPs was measured and it
236 was close to neutral: +1.26 ± 0.02 mV. Such a low potential suggests there would be minimal interaction with the
237 negatively charged alginate chains or polyphenol crystals. Moreover, the concentration MNPs spiked into the
238 alginate phase was low, i.e., 0.02 wt.% (wet weight). Considering the dry weight of the magnetic suspension was

239 only 0.19 ± 0.01 wt.%, the actual wt.% of iron oxides in the samples was only ~ 0.004 wt.%. At such low
240 concentrations, it is therefore not surprising that the MNPs did not significantly change the microgel particle
241 formation with or without polyphenols. However, another concern to address was whether the concentration of
242 MNPs was high enough to coat a significant fraction of the surface of the microgel particles and possibly inhibit
243 the entrapment of water-insoluble compounds. Assuming representative radii of the microgel and MNP as 5 μm
244 and 67 nm, respectively, then in 1 g of microgel suspension the ratio of the total surface area of the microgel
245 particles versus MNPs is calculated to be at least 100:1. Thus, the total surface area of the microgel particles far
246 exceeds the capacity of the MNPs to dominate this region of the microgels, even discounting the fact that at least
247 some of the MNPs are likely to be trapped within them.

248 *3.4. Microscopy of microgel-encapsulated systems*

249 The CLSM method benefited from the autofluorescence properties of rutin, tiliroside, curcumin and β-
250 carotene to highlight their positioning within the Ca-alginate microgel particles to visualize the success, or not, of
251 the encapsulation. The microgel particles do not fluoresce, but by adding the high molecular weight FITC-dextran,
252 that could not penetrate into the particles but remained in the continuous aqueous phase, negative contrast
253 images of the particles were obtained.

254 Representative CLSM images of Ca-ALG+CU and Ca-ALG+T are shown on Figure 5 (a and b). Bright
255 clusters of curcumin and tiliroside crystals are visible on the left which appeared coterminous with the dark
256 objects of the microgel particles on the right. This was a good direct evidence that clusters of insoluble organic
257 crystals were entrapped within the nascent of the microgel particles. Similar results were obtained with the other
258 water-insoluble compounds, including rutin and β-carotene (data not shown).

259 *3.5. Microgel Particle Yield*

260 The microgel particle yield was defined as the percentage weight of microgel particles separated
261 magnetically from the suspension as a fraction of the total weight of the suspension. The microgel yields are
262 reported in Figure 6a. When water-insoluble crystals were encapsulated, the microgel yield improved by at least

263 2-fold, ranging from 10.7 % to 29.4 %. The highest microgel yields were Ca-ALG+BC with or without TW 20, i.e.,
264 21.7 % and 29.4% respectively. Although there was a trend of lower microgel yield in Ca-ALG+BC+TW 20, the
265 result was not significantly different ($p > 0.05$). The microgel particle yields of Ca-ALG+R vs. Ca-ALG+CU were
266 20.8 % vs. 15.1 %, respectively, with no significance difference ($p > 0.05$). The microgel yield of Ca-ALG+T, i.e.,
267 10.7 %, was the lowest, with $p < 0.05$ compared to Ca-ALG+R. A plausible explanation for such an improvement
268 in microgel yield is that the insoluble particles serve as "nuclei" to initiate the formation of the microgel particles in
269 the turbulent mixing conditions in the jet homogenizer, as mentioned earlier.

270 The physical properties of the insoluble compounds, such as density, molecular weight (M_w) and particle
271 size, were considered to see if there was any correlation with the microgel yield. The microgel yield did not
272 correlate with the density order of the compounds (correlation coefficient was < 0.3). The density of tiliroside and
273 rutin are similar: 1.69 vs. 1.77 $g.ml^{-1}$, respectively, while the density of curcumin is 1.29 $g.ml^{-1}$. However the
274 microgel yield of tiliroside was the lowest, whilst the yields of rutin and curcumin were similar. The lack of
275 correlation with density suggests there was no significant gravitational separation occurring during the isolation of
276 the particles to determine their yield.

277 There was also no correlation of yield with the M_w of the compounds. The M_w of tiliroside and rutin are
278 similar: 594.53 and 664.58 $g.mole^{-1}$; the M_w of curcumin is 368.39 $g.mole^{-1}$. However, it should be remembered
279 that the encapsulation took place way above the solubility limit of these compounds, so that hardly any free
280 molecular polyphenol or curcumin were present. Thus it might be expected that microgel yield and M_w of the
281 insoluble materials are not related. Similarly, M_w the density of the compounds would not necessarily be
282 expected to show any relationship to the size of their insoluble crystals. For example, tiliroside had the highest
283 density and M_w close to that of rutin, but it easily had the smallest crystal size. Interestingly, it appeared that the
284 microgel yield *was* slightly correlated to particle size of the sub-micron 'nanocrystals' (see section 3.1) of the
285 insoluble materials (correlation coefficient 0.72): the smaller the particle size, the lower the microgel yield. The
286 particle size of the tiliroside crystals was 182.4 nm and resulted in lower yields than with rutin and curcumin. The
287 crystal sizes were approximately the same range for rutin and curcumin (~210 nm), and the microgel yields were

288 approximately the same for those two compounds. This is again possibly linked to an effect of the insoluble
289 crystals acting as 'nuclei' for microgel particle formation. Smaller crystals would suggest *more* nuclei would be
290 available and therefore greater yields, but at present it is not clear what mass faction of the polyphenols were
291 present as aggregates versus these nanocrystals during conditions of microgel particle formation.

292 *3.6. Payloads and Loading Efficiencies*

293 The payload is defined as the percentage weight of encapsulated compounds in the microgel particles as
294 a fraction of the weight of the microgel suspension. In general, the payloads were between 0.037 % to 1.2 % for
295 curcumin (the lowest) and the highest for β-carotene (BC) (0.61 % for Ca-ALG+BC and 1.2 % for Ca-
296 ALG+BC+TW20) – see Figure 6b. However, this difference was at least partly due to the higher initial
297 concentration of β-carotene than polyphenols in the original alginate solution used for encapsulation. There was
298 obviously a significant increase in the payload of BC as TW20 was introduced into the system ($p < 0.05$). TW20
299 is a non-ionic surfactant, with an HLB value of 16.7, commonly used as an O/W emulsifier. Here the BC was
300 present as crystals rather than oil droplets, but possibly the TW20 aided encapsulation in acting as a dispersant
301 for the hydrophobic BC crystals or altered their surface so that they had a greater affinity for the hydrophilic
302 microgel particles.

303 The same concentration (0.5 mM) of rutin, tiliroside and curcumin was loaded into the alginate phase
304 before microgel particle formation, thus the payloads can be more easily compared against each other. The
305 order of the payloads from the highest to the lowest was: Ca-ALG+T > Ca-ALG+R ≥ Ca-ALG+CU. The payload
306 of Ca-ALG+T was significantly higher ($p < 0.05$) than Ca-ALG+R and Ca-ALG+CU. Thus, the smaller tiliroside
307 crystals resulted in a higher payload (the correlation coefficient was -0.97), presumably because smaller crystals
308 are more easily trapped inside the microgel particles as they are formed. Thus, the particle size of the insoluble
309 crystals again seemed to be the dominant characteristic determining any effect on payload.

310 The payloads may be considered low if compared with the same compounds encapsulated via alternative
311 methods, such as spray drying, for example. Encapsulated curcumin in chitosan nanoparticle complex has been

312 studied elsewhere via spray drying and obtained payloads > 80 %.[26] However, the initial curcumin
313 concentration used in their work was 27 times higher than our current study. Moreover, the microgel particles in
314 our study are produced as a liquid suspension, not in the form of a powder. Drying naturally increases the
315 payload tremendously. Freeze-dried curcumin loaded microcapsules (yeast cells) had a considerably high
316 payload (around 10 % and 21% for curcumin in water and 50 vol.% ethanol, respectively), but again starting with
317 a much higher (5x) initial concentration of curcumin.[27]

318 Loading efficiency was also quantified to gauge the relative ease with which the different water-insoluble
319 compounds were trapped inside the microgel particles. Loading efficiency, sometimes referred to as
320 encapsulation efficiency, is defined as percentage weight of the encapsulated compounds found inside the
321 microgel particles as a fraction of the total weight of the encapsulated compounds added into the system. As
322 depicted from Figure 6c, the loading efficiencies of Ca-ALG+T and Ca-ALG+R were the highest, i.e., 57% and 58
323 % respectively, followed by Ca-ALG+CU, i.e., 37 %. The lowest loading efficiency was for β-carotene: Ca-
324 ALG+BC and Ca-ALG+BC+TW20 were 21.5 % and 30.9 % respectively, significantly lower ($p < 0.05$) compared
325 to the polyphenols mentioned above.

326 To try and explain why the encapsulation efficiency of the polyphenol crystals was much higher than the
327 hydrophobic β-carotene crystals, the charge density per unit surface area (μm^2) of the compounds was
328 estimated. One hypothesis was a higher charge density would produce a higher loading efficiency because there
329 would be more binding sites available to interact with the alginate. The maximum possible number of (-ve)
330 charges highlighted in the chemical structures of water-insoluble compounds is visually depicted in Figure 1. The
331 maximum number of electronic charges comes mainly from the hydroxyl groups at the surface of the crystals,
332 which could bind with alginate via Ca^{2+} ion cross-linking or via hydrogen bonding depending on the pH of the
333 system.

334 The charge densities were calculated based on the assumption that all the crystals were spherical and
335 that all the charges were exposed on the surface. On this basis, rutin and tiliroside possessed the highest charge
336 density, i.e., 28.7 charges.μm^{-2} for both. They also had the highest loading efficiency, i.e., 58 % for Ca-ALG+R

337 and 57 % for Ca-ALG+T. The loading efficiency of tiliroside was approximately the same as for rutin, despite
338 tiliroside having the smallest crystal size. The extra OH group in the flavone ring of rutin raises its charge density
339 to be on a par with tiliroside. However, there seems to be a significant lack of knowledge of the actual surface
340 charge distribution on flavonoid crystals surfaces that awaits further investigation.

341 **4. Conclusions**

342 The new technique of encapsulation of water-insoluble compounds in microgel particles produced via the
343 Leeds jet homogenizer has been demonstrated. Many mainstream approaches to fabricate gel particles such as
344 spray drying, prilling, or using proprietary encapsulators, produce high yields of particles but the sizes are
345 considerably larger (>1 um) than can be produced by the simple process outlined in this article. In the jet
346 homogenizer, the particle yields may considered to be low, but smaller particles can be produced. It was shown
347 that particle yield, payload and encapsulation efficiency seemed to be mainly dependent on the size and possibly
348 also the surface charge density of the particles being encapsulated, probably via the types of interaction that
349 enable them to bind with alginate. Loading with insoluble particles actually tended to improve the microgel yield.
350 High numbers of hydrogen bonding moieties in rutin and tiliroside gave the highest loading efficiency (> 50 %).
351 Payloads were low in this study but only because the initial concentration of compounds was low (0.5 mM for
352 polyphenols and 18.5 mM for β-carotene) in the starting solutions. Regardless of the low payloads, encapsulation
353 of water-insoluble compounds via the jet homogenizer showed high loading efficiencies which makes it a
354 technique worth pursuing further as a means of generating microgel particles for health and well-being functions.

355 **Acknowledgements**

356 The authors would like to acknowledge Mr. Phillip Bentley for the discussion of MNPs preparation. LCP also
357 acknowledges financial support for this work via a Leeds International Research Scholarship.

358 **References**

359 1. D.J. McClements, Designing biopolymer microgels to encapsulate, protect and deliver bioactive
360 components : Physicochemical aspects. *Advances in Colloid and Interface Science*, 2017, **240**, 31–59.
361 2. O. Torres, B. Murray, and A. Sarkar, Emulsion microgel particles: Novel encapsulation strategy for
362 lipophilic molecules, *Trends in Food Science and Technology*, 2016, **55***,* 98-108.
363 3. G. Galati and P.J. O'Brien, Potential toxicity of flavonoids and other dietary phenolics: Significance for
364 their chemopreventive and anticancer properties. *Free Radical Biology and Medicine*, 2004, **37**(3), 287–
365 303.
366 4. K Gul, A. Tak, A.K. Singh, P. Singh, B. Yousuf, & A.A. Wani, Chemistry, encapsulation, and health
367 benefits of Beta-carotene - A review. *Cogent Food & Agriculture*, 2015, **1**(1), 1–12.
368 5. M.A. Soobrattee, T. Bahorun, & O.I. Aruoma, Chemopreventive actions of polyphenolic compounds in
369 cancer. *BioFactors*, 2006, **27**(1-4), 19–35.
370 6. Z. Fang, and B. Bhandari, Encapsulation of polyphenols - a review. *Trends in Food Science and*
371 *Technology*, 2010, **21**(10), 510-523.
372 7. E. Acosta, Bioavailability of nanoparticles in nutrient and nutraceutical delivery. *Current Opinion in Colloid*
373 *& Interface Science*, 2009, **14**(1), 3–15.
374 8. L. De Souza, D.A. Madalena, A.C. Pinheiro, J.A. Teixeira, A.A. Vicente, & Ó.L. Ramos, Micro- and nano
375 bio-based delivery systems for food applications : In vitro behavior. *Advances in Colloid and Interface*
376 *Science*, 2017, **243**, 23–45.
377 9. L. Pravinata, M. Akhtar, P.J. Bentley, T. Mahatnirunkul, & B.S. Murray, Preparation of alginate microgels
378 in a simple one step process via the Leeds Jet Homogenizer. *Food Hydrocolloids*, 2016, **61**, 77–84.
379 10. A. Araiza-Calahorra, M. Akhtar, & A. Sarkar, Recent advances in emulsion-based delivery approaches for
380 curcumin: From encapsulation to bioaccessibility. *Trends in Food Science & Technology*, 2018, **71**, 155-
381 169.
382 11. Z. Luo, B.S. Murray, A.L. Ross, M.J.W. Povey, M.R.A. Morgan, & A.J. Day, Effects of pH on the ability of
383 flavonoids to act as Pickering emulsion stabilizers. *Colloids and Surfaces B: Biointerfaces*, 2012, **92**, 84–
384 90.
385 12. R. Mauludin, R.H. Müller, & C.M. Keck, Kinetic solubility and dissolution velocity of rutin nanocrystals.
386 *European Journal of Pharmaceutical Sciences*, 2009, **36**(4-5), 502–510.
387 13. H.H. Tønnesen, Solubility and stability of curcumin in solutions containing alginate and other viscosity
388 modifying macromolecules: Studies of curcumin and curcuminoids. *Pharmazie*, 2006, **61**(8), 696–700.
389 14. C.P. Coronel-Aguilera and M.F. San Martín-González, Encapsulation of spray dried β-carotene emulsion
390 by fluidized bed coating technology. *LWT - Food Science and Technology*, 2015, **62**(1), 187–193.
391 15. J. Garcia-Alonsoa, R.F. Fakhrullin, & V.N. Paunov, Rapid and direct magnetization of GFP-reporter yeast
392 for micro-screening systems. *Biosensors and Bioelectronics*, 2010, **25**(7), 1816–1819.

393 16. O. Torres, B. Murray, & A. Sarkar, Design of novel emulsion microgel particles of tuneable size. *Food*
394 *Hydrocolloids*, 2017, **71**, 47–59.
395 17. O. Torres, N.M. Tena, B. Murray, & A. Sarkar, Novel starch based emulsion gels and emulsion microgel
396 particles: Design, structure and rheology. *Carbohydrate Polymers*, 2017, **178**, 86–94.
397 18. K. Matsumiya and B.S. Murray, Soybean protein isolate gel particles as foaming and emulsifying agents.
398 *Food Hydrocolloids*, 2016, **60**, 206–215.
399 19. B.S. Murray & N. Phisarnchananan, Whey protein microgel particles as stabilizers of waxy corn starch +
400 locust bean gum water-in-water emulsions. *Food Hydrocolloids*, 2016, **56**, 161–169.
401 20. Y. Li, M. Hu, Y. Du, H. Xiao, & D.J. McClements, Control of lipase digestibility of emulsified lipids by
402 encapsulation within calcium alginate beads. *Food Hydrocolloids*, 2011, **25**(1), 122–130.
403 21. K.Y. Lee and D.J. Mooney, Alginate: properties and biomedical applications. *Progress in Polymer*
404 *Science*, 2012, **37**(1), 106–126.
405 22. Z. Zhang, R. Zhang, L. Chen, Q. Tong, & D.J. McClements, Designing hydrogel particles for controlled or
406 targeted release of lipophilic bioactive agents in the gastrointestinal tract. *European Polymer Journal*,
407 2015, **72**, 698–716.
408 23. Z. Wang, M.H.M. Leung, T.W. Kee, & D.S. English, The role of charge in the surfactant-assisted
409 stabilization of the natural product curcumin. *Langmuir*, 2010, **26**(8), 5520–5526.
410 24. J.M. Herrero-Martínez, M. Sanmartin, M. Rosés, E. Bosch, & C. Ràfols, Determination of dissociation
411 constants of flavonoids by capillary electrophoresis. *Electrophoresis*, 2005, **26**(10), 1886–1895.
412 25. L. Salvia-Trujillo, C. Qian, O. Martín-Belloso, & D.J. McClements, Influence of particle size on lipid
413 digestion and β-carotene bioaccessibility in emulsions and nanoemulsions. *Food Chemistry*, 2013,
414 **141**(2), 1475–1480.
415 26. M.H. Nguyen, H. Yu, T.Y. Kiew, & K. Hadinoto, Cost-effective alternative to nano-encapsulation:
416 Amorphous curcumin-chitosan nanoparticle complex exhibiting high payload and supersaturation
417 generation. *European Journal of Pharmaceutics and Biopharmaceutics*, 2015, **96**, 1–10.
418 27. E.I. Paramera, S.J. Konteles, & V.T. Karathanos, Microencapsulation of curcumin in cells of
419 Saccharomyces cerevisiae. *Food Chemistry*, 2011, **125**(3), 892–902.

420 **Figure Legends**

421 **Figure 1.** Chemical structures of water-insoluble materials encapsulated. Potential ionizable (negative) groups
422 and their maximum number (N) are highlighted.

423 **Figure 2.** PSD of rutin, tiliroside, curcumin (1 mM dispersed in water) and Ca-alginate microgel particles
424 prepared from 20 mM Ca2+ and 2 wt.% of alginate in 0.02 M of imidazole buffer pH 5 and 8.

425 **Figure 3.** (a) Particle Sauter mean diameter ($d_{3,2}$) of Ca-alginate microgel particles with or without the insoluble
426 polyphenols at pH 5 and 8 (b) the ζ-potentials of Ca-alginate microgel particles with and without flavonoids at pH
427 5 and 8 in 0.02 M imidazole buffer.

428 **Figure 4.** Particle size of β-carotene crystals stabilized with TW20 dispersed in water after mixing at 24,000 rpm
429 via the Ultraturrax (___), added with 2 wt.% alginate (— —), homogenized and encapsulated in microgel particles
430 (…).

431 **Figure 5.** Micrographs of 0.5 mM curcumin (a) and 0.5 mM tiliroside (b) entrapped in Ca-alginate microgel
432 particles obtained from CLSM excited at 458 nm (left side) and 488 nm (right side).

433 **Figure 6.** (a) Microgel yield of Ca-alginate microgel particles including MNPs (0.02 %wt. concentration) with and
434 without the encapsulated water-insoluble compounds and the correlation with the polyphenol crystal sizes
435 displayed as an inset figure, (b) Payloads of the encapsulated microgel particles, (c) Loading efficiencies of
436 encapsulated microgel particles and the correlation with the charge densities of the crystals displayed as an inset
437 figure.

438

Figure 1

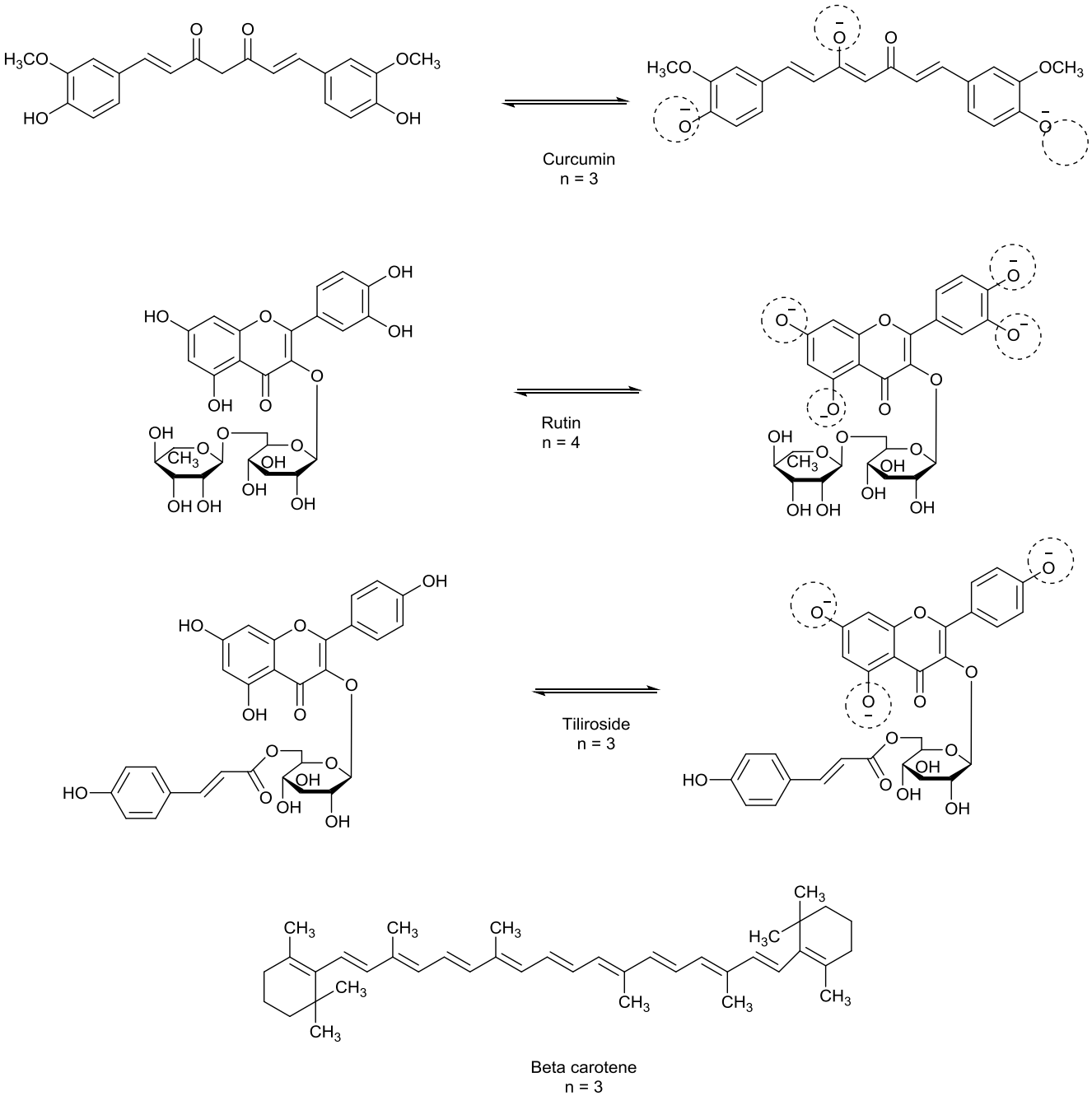

442 **Figure 2**

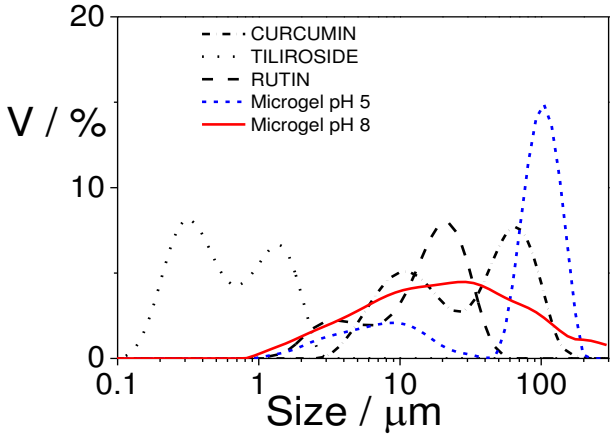

443

Figure 3

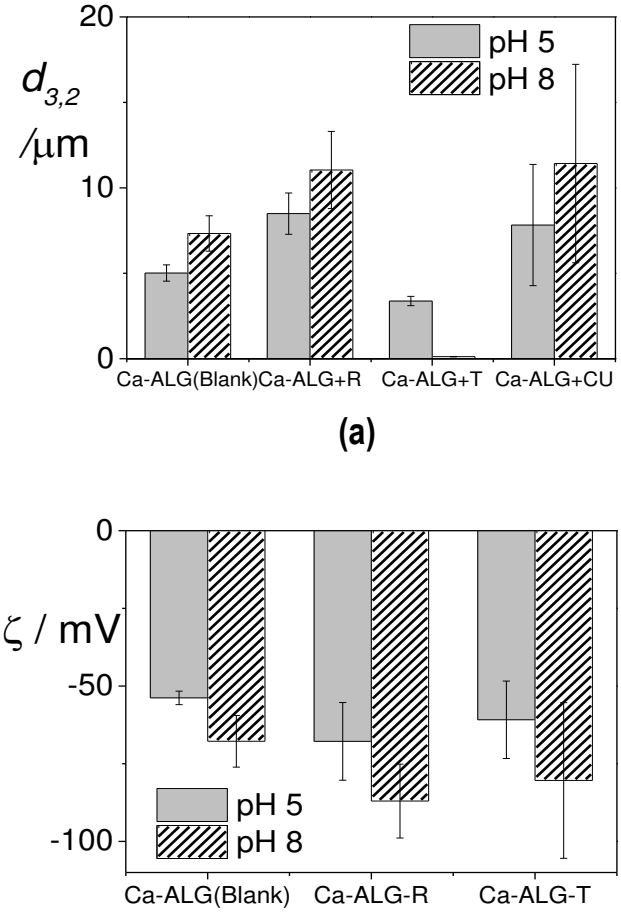
20
10
0
$d_{3,2}$
/μm
pH 5
pH 8
Ca-ALG(Blank)
Ca-ALG+R
Ca-ALG+T
Ca-ALG+CU
(a)
0
-50
-100
ζ / mV
pH 5
pH 8
Ca-ALG(Blank)
Ca-ALG-R
Ca-ALG-T

447 **Figure 4**

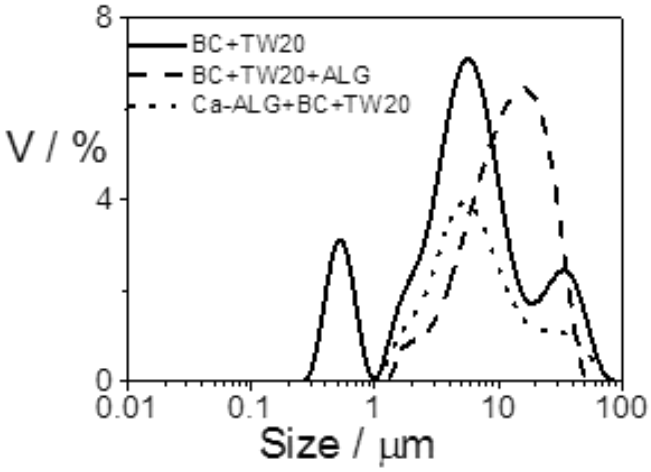

448

449 **Figure 5**

450

451 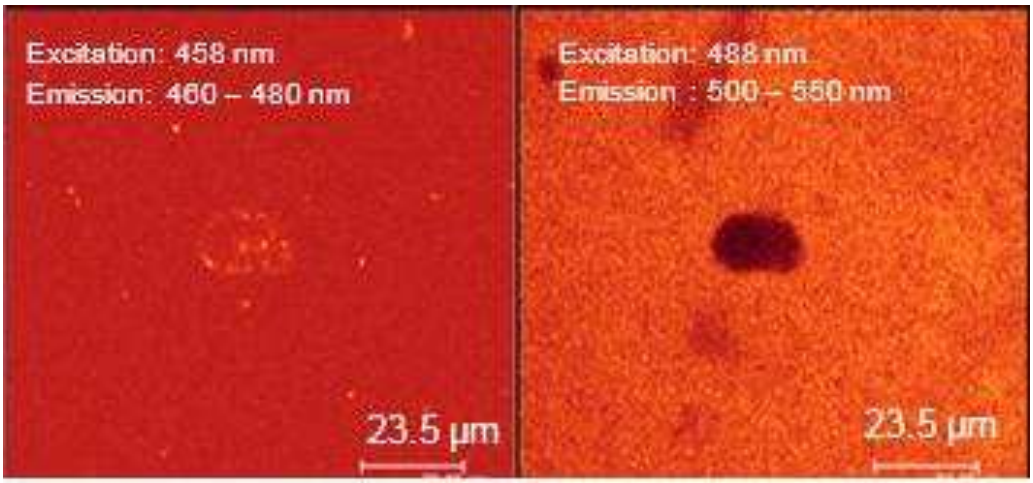

452 **(a)**

453 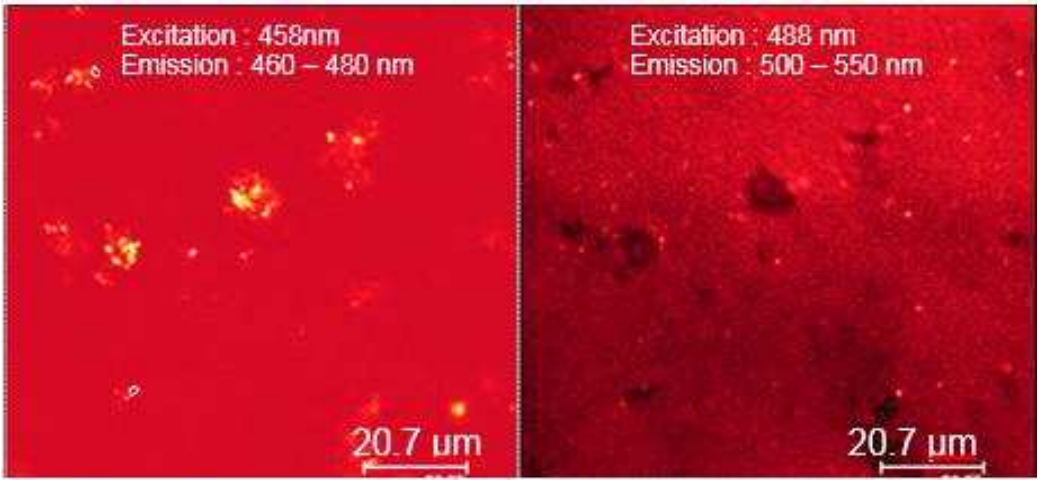

454 **(b)**

455

Figure 6

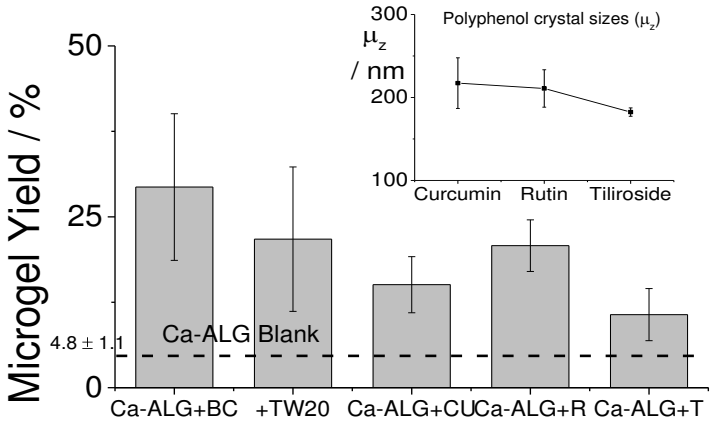
Microgel Yield / %
50
25
0
4.8 ± 1.1
Ca-ALG Blank
Ca-ALG+BC
+TW20
Ca-ALG+CU
Ca-ALG+R
Ca-ALG+T
Polyphenol crystal sizes (μ_z)
300
μ_z
/ nm
200
100
Curcumin
Rutin
Tiliroside

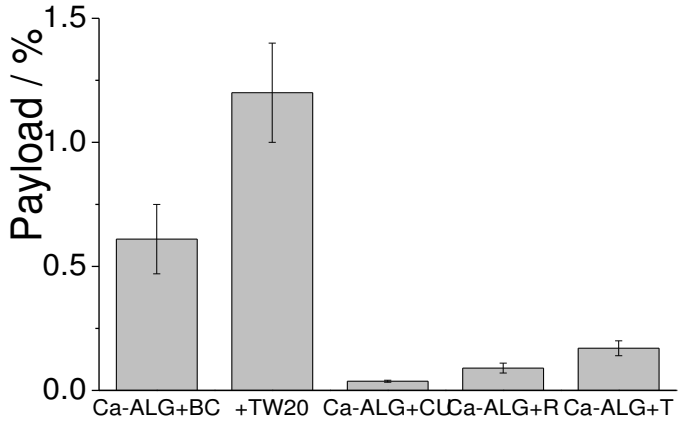
Payload / %
1.5
1.0
0.5
0.0
Ca-ALG+BC
+TW20
Ca-ALG+CU
Ca-ALG+R
Ca-ALG+T

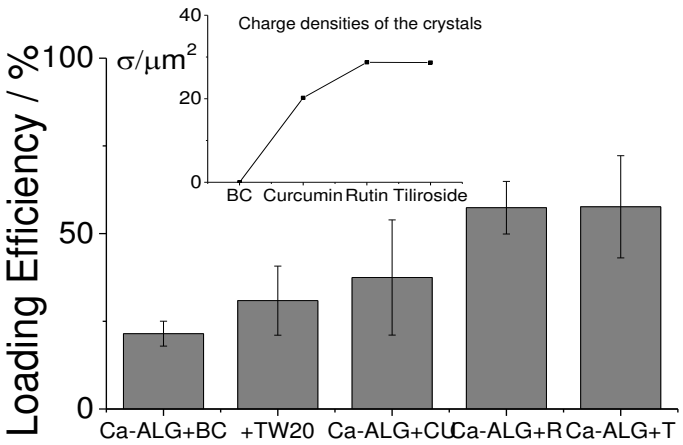
Loading Efficiency / %
100
50
0
Ca-ALG+BC
+TW20
Ca-ALG+CU
Ca-ALG+R
Ca-ALG+T
Charge densities of the crystals
40
$\sigma/\mu m^2$
20
0
BC
Curcumin
Rutin
Tiliroside

Abstract

Polyphenols and β-carotene are widely studied due to their perceived multiple health functions, but their poor solubility in water inhibits their addition to foodstuffs. This provides a motivation for this study: to entrap these water–insoluble compounds into Ca-alginate microgel particles prepared via a special technique termed the Leeds Jet Homogenizer. Water-insoluble particles of polyphenols and β-carotene were successfully loaded into the microgel particles as revealed by images obtained from confocal laser scanning microscopy (CLSM). Microgel particles were separated via incorporation of magnetic nanoparticles (MNPs) into the particles and application of a magnetic field or via centrifugation, to quantify the yield, payload, and loading efficiencies. It was found that microgel particle yields improved on introducing these water-insoluble compounds up to 10 % to 30 %. The payloads of compounds in the particles were only < 1.5 % but mainly due to the low initial concentrations were used, i.e. 0.5 and 18.5 mM for polyphenols and β-carotene, respectively. The loading efficiencies were considerably high, i.e. between 21 to 58 %. In short, the results show firm evidence that useful encapsulation of such water-insoluble compounds within Ca-alginate microgel particles can be achieved via this simple and effective technique.

***Graphical Abstract (for review)**